Research Article

Eman Aldosari, Mohamed Rabia*, Aimaro Sanna, and Osama Farid*

Single-step fabrication of Ag_2S/poly-2-mercaptoaniline nanoribbon photocathodes for green hydrogen generation from artificial and natural red-sea water

https://doi.org/10.1515/phys-2024-0095
received September 01, 2024; accepted October 29, 2024

Abstract: A novel and highly promising Ag_2S-P2MA nanoribbon photocathodes are synthesized using a single-step technique based on 2-mercaptoaniline oxidation with $(NH_4)_2S_2O_8$ and $AgNO_3$. This process yields polymer composites with nanoribbon morphologies, typically 150 nm wide and ranging from 500 to 1,000 nm in length. These nanoribbons exhibit excellent absorbance across the entire optical spectrum up to 780 nm. The fabricated Ag_2S/P2MA photocathode is designed for water splitting to generate hydrogen gas using two different electrolytes: natural Red Sea water and artificial seawater free from heavy metals. This variation allows observation of the impact of seawater's heavy metals. Hydrogen gas production is studied using a three-electrode cell with linear sweep voltammetry at room temperature. In both electrolytes, the photocurrent is measured at 0.015 mA/cm^2. However, both the current density in light (J_{ph}) and dark (J_o) values decrease in artificial seawater compared to natural seawater, with values of −0.033 and −0.017 mA/cm^2 in natural seawater and −0.027 and −0.012 mA/cm^2 in artificial seawater. The Ag_2S-P2MA nanoribbon photocathodes exhibit stable behavior, producing hydrogen at a rate of 12 μmol/cm^2 h. Combined with their cost-effectiveness and potential for mass production, this positions them as viable candidates for commercial electrode applications in various industrial settings.

*** Corresponding author: Mohamed Rabia**, Nanomaterials Science Research Laboratory, Chemistry Department, Faculty of Science, Beni-Suef University, Beni-Suef, 62514, Egypt,
e-mail: mohamedchem@science.bsu.edu.eg
*** Corresponding author: Osama Farid**, Reactor Department, Nuclear Research Centre, Egyptian Atomic Energy Authority (EAEA), P.O. Box 13759, Inshass, Cairo, Egypt, e-mail: usamafa98@hotmail.co.uk
Eman Aldosari: Department of Chemistry, College of Science, King Saud University, P.O. Box 145111, Riyadh, Saudi Arabia
Aimaro Sanna: School of Engineering & Physical Science, Heriot-Watt University, Edinburgh, United Kingdom

Keywords: poly-2-mercaptoaniline, nanoribbon, green hydrogen, photocathode, renewable energy

1 Introduction

The global energy crisis, particularly due to increasing pollution and the dwindling supply of fossil fuels, has significantly heightened the demand for clean, environmentally friendly energy. Fossil fuels, which are currently a major source of the world's electricity, contribute significantly to atmospheric pollution, leading to global warming. As a result, there is a growing urgency to shift toward renewable energy sources, with hydrogen gas emerging as one of the most viable and widely used options [1,2].

Hydrogen (H_2) gas is considered the most cost-effective and extensively utilized renewable energy source. Scientists are capable of producing H_2 through photocatalysis from a range of electrolytes, including acidic, basic, and neutral media. This method of production is particularly valuable as hydrogen gas is increasingly being adopted by numerous factories and companies as a cleaner alternative to fossil fuels. By reducing the reliance on fossil fuels, the emission of harmful gases such as sulfur oxides, nitrogen oxides, and carbon dioxide is also minimized, thereby lessening their detrimental impact on the environment. Additionally, H_2 gas demonstrates excellent combustibility and performance, making it an attractive candidate for a sustainable energy source [3,4]. However, the widespread use of hydrogen gas as a clean and sustainable fuel in the future hinges on great efficient photocatalysts. The generation of H_2 gas through water electrolysis faces a significant challenge due to the sluggish oxygen evolution reactions, which require a voltage >1.23 V for the process to occur efficiently. This necessitates the exploration of more effective methods to produce hydrogen [5–7].

One promising approach to mitigate the current energy crisis is the production of hydrogen gas through photocatalysis

and direct water splitting. This process involves the use of metal sulfides or polymer materials that possess excellent optical properties. These materials are not only beneficial in light-induced reactions but also offer commercial advantages such as the potential for mass production and cost-effectiveness [8,9]. The effectiveness of these materials in producing H_2 gas is largely attributed to their large surface areas, which provide numerous active sites for the reaction. Nanomaterials, nanowires, or nanosheets, in particular, are advantageous because they enhance the efficiency of hydrogen generation by active sites available for the reaction. Improvement in the material's structural design is crucial for maximizing the production of hydrogen gas, thus making it a more feasible and sustainable alternative to fossil fuels [10,11]. Various applications have been proposed to address this issue, particularly in the field of materials science. Transition metal oxides are employed in the doping process for a range of materials, including carbon-based substances, noble metals, nonmetals, as well as both homo- and heterostructures. These materials are especially significant in electrical devices where polymers are used to create metal-substitutable compounds. The researchers' aim in synthesizing polymers with an optimal band gap between 1.2 and 1.5 eV, which is crucial for enhancing photon absorption within the molecular structure of these materials [12,13].

Advancements in this area include the development of nanoformulations and composites that utilize additives with a wide spectrum of light-responsive properties. These innovations demonstrate significant progress in the field. Research efforts have also focused on polymer compounds aimed at producing hydrogen gas and facilitating water splitting. However, the predominant methods employed are highly complex and often rely on electrolytes made from harsh, basic, or acidic materials. This approach can lead to increased corrosion within the cells used for these processes, posing a challenge for long-term application and efficiency [14].

Herein, a novel one-pot technique was employed to synthesize Ag_2S-P2MA nanoribbon photocathodes. Characterization using SEM and TEM studies revealed the nanoribbons in these nanocomposites, while optical absorbance and analyses such as XRD, FTIR, and XPS provided insights into their optical and chemical structures. These photocathodes were specifically designed for generating hydrogen gas through water splitting using two types of electrolytes: natural Red-sea water and artificial seawater without heavy metals. Testing under various optical conditions demonstrated their efficacy across different energy levels. With their significant hydrogen gas generation, cost-effectiveness, stability, and potential for large-scale production, these photocathodes are highly suitable for commercial electrode applications in diverse industrial sectors.

2 Materials and methods

2.1 Materials

2-Mercaptoaniline (99.9%) (P2MA) was obtained from Germany (Merck Co.). Silver nitrate ($AgNO_3$, 99.9%), ammonium persulfate ($(NH_4)_2S_2O_8$, 99.8%), CH_3COOH (99.8%), and HCl (36%) were procured from Egypt (Pio-Chem Co.). DMF was supplied by Sigma Aldrich Co., USA.

2.2 One-pot synthesis of the Ag_2S/P2MA nanocomposite

The synthesis of the Ag_2S/P2MA nanocomposite was conducted using a one-pot technique involving the oxidation of 2-mercaptoaniline with $(NH_4)_2S_2O_8$ and $AgNO_3$. In this process, Ag_2S was incorporated within the polymer chains to form Ag_2S/P2MA. Initially, 0.06 M 2-mercaptoaniline was vigorously dissolved in 12 ml of CH_3COOH. Subsequently, 0.07 M $AgNO_3$ was added under continuous stirring for 30 min. In parallel, 0.15 M $(NH_4)_2S_2O_8$ was dissolved separately. The sudden reaction of the oxidant with the monomer solution initiated the polymerization reaction, resulting in the formation of the Ag_2S/P2MA composite. During this addition, a glass slide was inserted, allowing the formation of a composite. This film was then prepared for application within a three-electrode cell intended for the green gas generation reaction.

2.3 Ag_2S/P2MA nanoribbon photocathode for green H_2 generation

The behavior of the synthesized Ag_2S/P2MA nanoribbon photocathode for generating green hydrogen gas is investigated using a three-electrode cell setup. The Ag_2S/P2MA photocathode, formed as a thin film (main electrode), supplies electrons for the reduction of natural Red Sea water and an equivalent artificial seawater. The artificial seawater, which lacks metal ions, emphasizes the various ions impact present in Red Sea water, in Hurghada City, Egypt. The artificial seawater consists of NaCl, $CaCl_2$, $MgCl_2$, Na_2SO_4, and $KHCO_3$ at concentrations of 38.38, 2.43, 19.06, 5.26, and 0.24 g/l, respectively [15].

To complete the electrochemical cell, a calomel reference electrode and a graphite counter electrode are added. All experiments are conducted at 25°C using the CHI608E device. The device is utilized to measure linear sweep voltammetry and chronoamperometry, which are critical for

evaluating the photocurrent density (J_{ph}), indicative of the hydrogen gas generation efficiency.

These measurements are performed under different lighting conditions, including full-spectrum light and certain specific monochromatic lights based on sources used to provide specific photon energies achieved by employing optical filters. The photon energies tested include 3.6, 2.8, 2.3, and 1.8 eV. Through this comprehensive approach, the efficiency and behavior of the Ag_2S/P2MA nanoribbon photocathode in hydrogen production are analyzed, considering the influence of light conditions and the presence of heavy metals. The hydrogen produced is determined using the Faraday equation (Eq. (1)) [16]. This equation takes into account the oxidation states of hydrogen gas and its molecular weight, and it primarily relies on the values of the photocurrent density (J_{ph}).

$$H_2 \text{ mole} = \int_0^t J_{ph} \cdot dt/F. \quad (1)$$

3 Results and discussion

3.1 Analyses

Figure 1(d) presents the FT-IR spectra of P2MA and the Ag_2S/P2MA nanocomposite. In the P2MA spectrum, a stretching peak for N–H and S–H is observed at 3,366/cm. Additional spectral data further validate the structures, as shown in the spectra. Aromatic C–C stretching is also observed at 1,619 and 1,514/cm, with varying values across the spectra. Additionally, the C–N band is identified at 1,310/cm.

For the Ag_2S/P2MA nanocomposite, peaks are observed at 3,397, 1,200, 1,628, 1,401, and 1,089/cm, indicating the presence of the nanocomposite. The correlation between these peaks and the corresponding groups is detailed in Table 1. A notable difference is the Ag–O position, which exhibits a high-intensity peak within the composite, contrasting with the small and limited band observed in pristine P2MA.

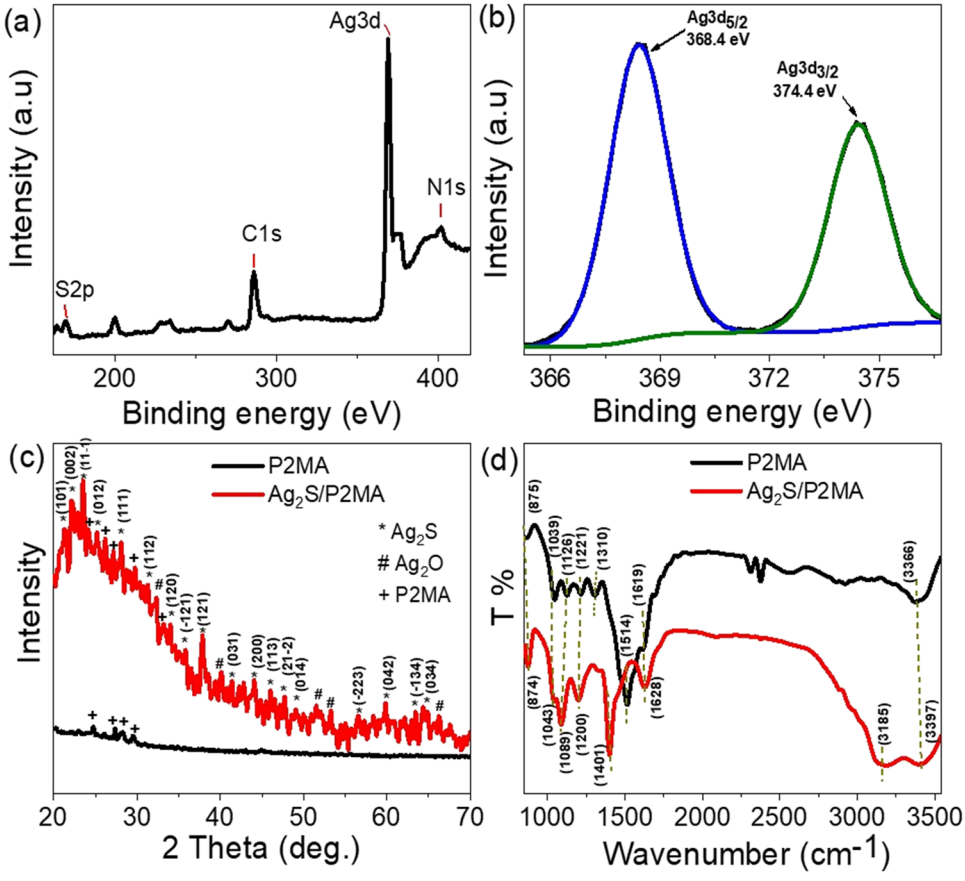

Figure 1: Chemical analyses of the synthesized Ag_2S/P2MA nanocomposite using the (a) XPS survey, (b) XPS Ag3d, (c) XRD pattern, and (d) FTIR spectroscopy.

Table 1: FTIR analysis of band positions: comparison of the Ag_2S/P2MA nanocomposite with P2MA polymer

Functional group	Group and its value (/cm)	
	Ag_2S/P2MA	P2MA
N–H [17]	3,397	3,366
Ag–S and C–H out of plane	875	874
C–H group [18]	1,200	1,126 and 1,221
C–N	1,400	1,310
C–C	1,628	1,514 and 1,619

The chemical composition of the synthesized Ag_2S/P2MA nanocomposite is assessed by evaluating the oxidation states and the constituent elements using XPS analysis (Figure 1(a) and (b)) for the survey and Ag 3d orbital, respectively. The survey spectrum verifies the presence of all polymer constituents, detecting the elements sulfur (S), carbon (C), and nitrogen (N) through their respective orbitals. Specifically, sulfur is identified by its 2p orbital at a binding energy of 165 eV, carbon by its 1s orbital at 286 eV, and nitrogen by its 1s orbital at 400 eV. Additionally, the presence of silver (Ag) is confirmed through its 3d orbitals, with $Ag3d_{5/2}$ and $Ag3d_{3/2}$ exhibiting binding energies of 368.4 and 374.4 eV, respectively [19,20]. These binding energies are consistent with the formation of silver sulfide (Ag_2S), validating the synthesis of the Ag_2S/P2MA composite.

For a comprehensive analysis of the synthesized Ag_2S/P2MA composite, the XRD pattern shown in Figure 1(c) reveals the formation of crystalline peaks, demonstrating the excellent crystalline properties of the entire composite. The observed peaks for Ag_2S at 21.3°, 22.1°, 23.7°, 25.1°, 28.2°, 31.2°, 34.1°, 35.9°, 37.9°, 41.3°, 44.2°, 46.1°, 47.6°, 49.0°, 56.5°, 59.8°, 63.5°, and 64.3° correspond to the growth directions (101), (002), (11-1), (012), (111), (112), (120), (-121), (121), (031), (200), (113), (21-2), (014), (-223), (042), (-134), and (034), respectively [21]. Additionally, other peaks detected at 32.3°, 40.1°, 51.6°, 53.2°, and 66.1° indicate the presence of Ag_2O traces within the composite. Ag_2O traces contribute to enhanced electrical conductivity and photoabsorbance of the synthesized nanocomposite [22].

Pristine P2MA exhibits four semi-sharp peaks reflecting its semiconducting nature. These peaks are found in the range of 24.6°–29.5°. However, when P2MA is integrated into the composite, these peak shifts are observed in the range of 24.5°–33.5°, indicating the formation of more crystalline materials. Using the Scherrer equation (Eq. (2)) [23,24], the crystalline size (D) is estimated to be 70 nm, based on the peak at 2θ = 22.1°:

$$D = 0.9\lambda/\beta \cos \theta. \quad (2)$$

This equation considers the full width at half-maximum of this peak. The XRD analysis thus confirms the successful synthesis of the Ag_2S/P2MA composite with well-defined crystalline properties. The integration of P2MA into the composite and the presence of Ag_2O traces enhances the material's overall electrical and photoresponsive characteristics. The detailed peak analysis underscores the high crystalline quality and the formation of specific crystallographic orientations, which are essential for the composite's performance in various applications.

The morphology of the synthesized Ag_2S/P2MA nanocomposite is shown in Figure 2. The SEM image in Figure 2(a) provides the formation of nanoribbons, resulting from the interaction between Ag_2S and P2MA within the composite material. These nanoribbons have a width of approximately 150 nm and lengths varying from 500 to 1,000 nm. Each larger ribbon is composed of small, semispherical particles with an average diameter of 150 nm. The impressive morphology of these nanoribbons includes significant porosity between the particles, which, combined with their geometric structure, results in a large surface area [16,25]. The TEM images in Figure 2(c) and (d) provide a clearer view of the nanoribbons under various morphologies. These images reveal that the nanoribbons consist of tiny particles that aggregate to form a network, enhancing the structural integrity of the nanocomposite. This network-like structure contributes to the overall functionality of the composite by providing a robust and interconnected framework. In contrast, the pristine P2MA polymer displays a porous, spherical morphology, with diameters ranging from 250 to over 1,000 nm, as shown in Figure 2(b). This inherent porosity is advantageous for composite formation, as it facilitates interactions with additional materials during the reaction process. Overall, the SEM and TEM analyses highlight the distinctive morphologies of both the Ag_2S/P2MA nanocomposite and pristine P2MA polymer. The nanoribbons formed in the composite exhibit significant porosity and surface area, essential for enhancing the material's performance in various applications. The spherical, porous structure of pristine P2MA further underscores its potential as a component in composite materials, promoting effective integration and interaction with other substances.

The optical behavior of the synthesized Ag_2S/P2MA nanocomposite compared to the pristine P2MA polymer is measured using UV, as illustrated in Figure 3(a). The nanocomposite shows promising optical absorbance, covering a significant portion of the optical spectrum up to approximately 780 nm. This makes the Ag_2S/P2MA nanocomposite an excellent material for photon trapping and capture, facilitated by its porous structure and produced

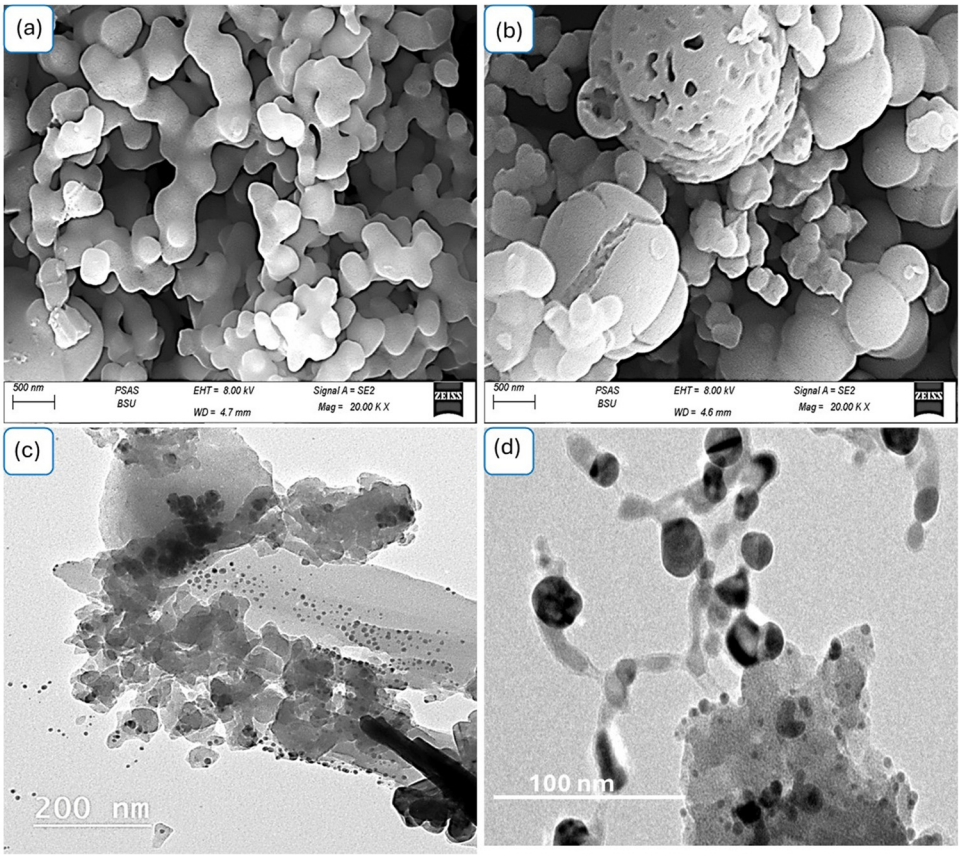

Figure 2: Morphological analyses of the synthesized Ag_2S/P2MA nanocomposite: (a) SEM and (c, d) TEM images at various magnifications, and (b) the SEM image of the pristine polymer P2MA.

nanoparticles. The wide absorbance range indicates efficient electron transfer to the upper conducting level upon photon incidence, occurring in both the UV and visible regions. These transferred electrons form a dense cloud, generating an electric field on the surface of the composite material [26,27].

As the absorbance extends into the IR region, it reflects electron bond vibrations rather than electron transfer due to the lower energy of the IR spectrum. In contrast, the pristine P2MA polymer exhibits lower intensity and a narrower coverage spectrum, extending only to 600 nm, which is a limited spectrum and short compared to the composite material.

The difference in behavior is also evident in the bandgap values, with the composite having a bandgap of 2.16 eV, while the pristine polymer's bandgap is 2.76 eV, as shown in Figure 3(b). Using Eq. (3) (Tauc equation) [28,29], the bandgap is evaluated, using the absorption coefficient (α) as the primary factor:

$$\alpha h\nu = A(h\nu - E_g)^{1/2}. \quad (3)$$

The smaller bandgap of the composite material contributes to its superior photon trapping and electron transfer capabilities, enhancing its overall optical performance.

3.2 Green hydrogen generation using a fabricated Ag_2S/P2MA thin film nanoribbon photocathode from natural/artificial seawater

Green hydrogen generation is carried out using a fabricated Ag_2S/P2MA thin film nanoribbon photocathode, employing either natural or artificial seawater. Red Sea water, with its unique chemical composition outlined earlier, is used as the electrolyte in this study. This selection offers significant benefits, primarily because it is environmentally sustainable and comes at no cost. A crucial factor in this process is the presence of ions in the seawater, which plays an important role in enhancing the electrolysis reaction. Under the used potential, these ions exhibit increased mobility, which

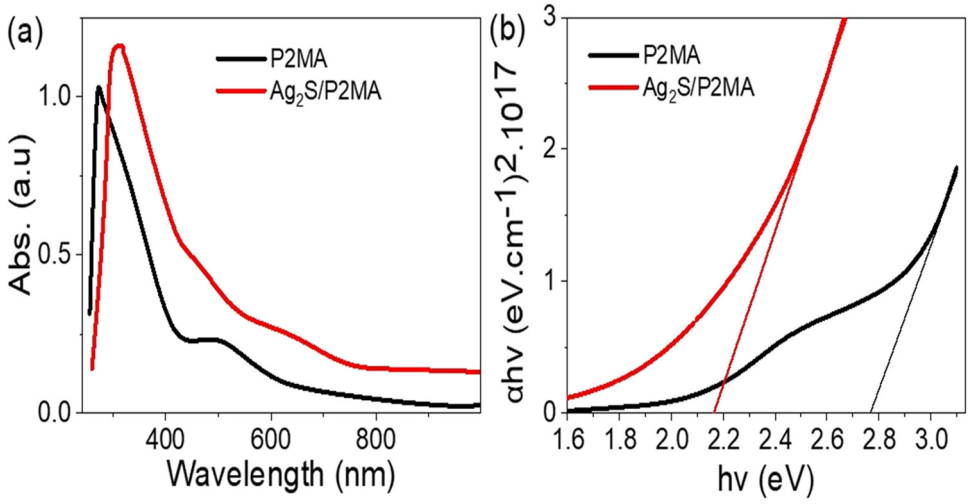

Figure 3: Comparison of the absorbance of the synthesized Ag_2S/P2MA composite relative to pristine P2MA, shown by the (a) absorbance spectrum and (b) bandgap evaluation.

contributes to the water-splitting process. The interaction of these metals with the electric field aids in facilitating the electrochemical reaction, improving the overall efficiency of hydrogen gas generation. Additionally, the natural abundance and availability of Red Sea water make it an ideal choice for large-scale applications, as it reduces the need for synthetic electrolytes, thus minimizing costs and environmental impact. By capitalizing on the inherent properties of Red Sea water, this approach provides a promising route for advancing energy production technologies that are both efficient and eco-friendly.

The entire process hinges on the photocatalytic properties of the Ag_2S/P2MA nanocomposite. The synergistic catalytic behavior of these two materials is essential for the photocatalytic activity. Their combined properties enhance photon trapping due to the porous structure of the materials. Furthermore, the small bandgap of 2.16 eV aids in the efficient transfer of electrons, which are then collected in the nanocomposite upper level. These electrons act as active agents, attacking neighboring molecules in the solution and driving the hydrogen gas generation process.

The unique properties of the Ag_2S/P2MA nanocomposite facilitate a series of reactions crucial for hydrogen generation. Its small bandgap allows it to efficiently absorb and utilize light, promoting the transfer of electrons. These electrons, once collected in the conducting band, are highly reactive and play a pivotal role in initiating the water-splitting reaction. The porous nature of the material not only enhances its ability to trap photons but also increases the surface area available for catalytic reactions, thereby improving the overall efficiency [30,31].

Utilizing Red Sea water as an electrolyte introduces an eco-friendly and cost-effective component into the system. The chemical composition of seawater, including various heavy metals, contributes to the mobility of ions during the application of the potential. Ion mobility is crucial for the electrolysis process, which splits water molecules into hydrogen and oxygen. Heavy metals present in seawater move within the electrolyte solution, facilitating the electrolysis reaction and subsequently leading to hydrogen gas generation. Figure 4(a) illustrates the exceptional photocatalytic performance of the Ag_2S/P2MA nanoribbon photocathode. The generated photocurrent is 0.015 mA/cm^2, resulting from the difference in current densities between light and dark conditions. Specifically, the photocurrent density (J_{ph}) is −0.034 mA/cm^2, while the dark current density (J_o) is −0.019 mA/cm^2, measured at an applied bias voltage of −0.6 V. This impressive performance in water splitting using seawater, without any additional electrolyte, highlights the superior photocatalytic properties of the Ag_2S/P2MA nanocomposite, which exhibits high sensitivity to incident photons. The sensitivity of this photocatalytic material is further demonstrated in Figure 4(b), which shows the chopped behavior of the Ag_2S/P2MA nanocomposite. The high responsivity to variations in J_{ph} values indicates its strong photocatalytic nature. This curve also showcases the stability and reproducibility of the Ag_2S/P2MA nanocomposite. Both the inorganic component Ag_2S and the polymer P2MA contribute to this stability. The polymer, in particular, provides anticorrosion resistance, ensuring that the produced current density remains consistently stable over time.

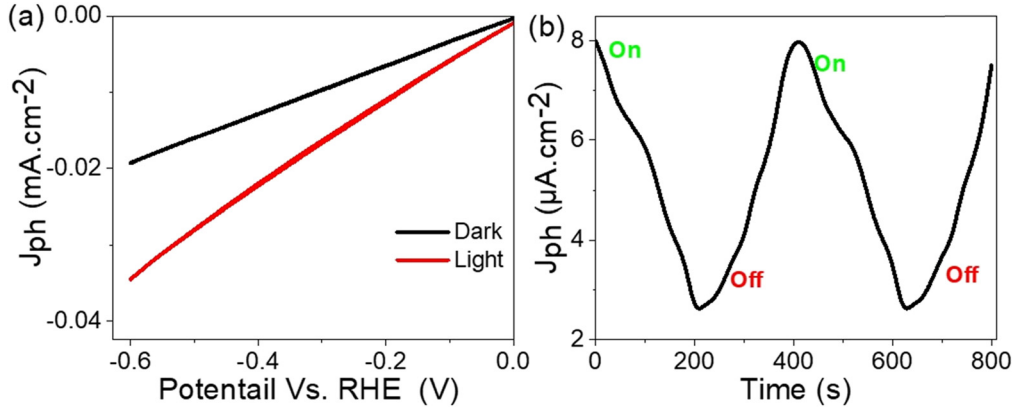

Figure 4: Green hydrogen generation using the fabricated Ag2S/P2MA thin film nanoribbon photocathode with natural Red Sea water: (a) linear sweep potentiometry and (b) chopped current under different optical light conditions.

To further assess the photocatalytic sensitivity of the fabricated Ag_2S/P2MA thin film photocathode for green hydrogen provided from Red Sea water, the effect of light wavelength on the photocathode was investigated, as shown in Figure 5(a). Using linear sweep voltammetry, the resulting current densities varied according to the photon energy, ranging from −0.033 to −0.028 mA/cm^2 as the light wavelengths decreased from 730 to 340 nm, respectively. Figure 5(b) presents this behavior in column form, highlighting the different responses of the photocathode to various photon energies. As photon wavelengths increase, their energies decrease, leading to a reduction in the photocathode's efficiency for gas generation, as indicated by the J_{ph} values. This is based on the kinetic energies of the hot electrons, which increase with higher photon energies. These electrons accumulate as dense clouds on the surface of the Ag_2S/P2MA nanoribbon photocathode, enhancing its capability to interact with the surrounding solution and generate hydrogen gas. As the photon energy decreases (with increasing wavelength), the kinetic energy of the electrons diminishes, resulting in reduced photocatalytic activity for hydrogen generation.

To ensure that heavy metals contribute to mobility as an electrolyte without consuming charges and thereby affecting the electrolysis process, artificial seawater free from these heavy metals was prepared. This approach allowed for the observation of the inherent photocatalytic behavior of the Ag_2S/P2MA thin film nanoribbon photocathode, as shown in Figure 6(a). The produced photocurrent in this setup is −0.015 mA/cm^2, similar to that observed with natural Red Sea water. However, there is a decrease in the current density values, with J_{ph} and J_o being −0.027 and −0.012 mA/cm^2, respectively. This demonstrates that the ions in Red Sea water play a crucial role in effectively activating the hydrogen gas generation reaction without consuming additional charges from the applied potential [3].

To quantify the hydrogen gas produced by the Ag_2S/P2MA thin film nanoribbon photocathode, Faraday's law of

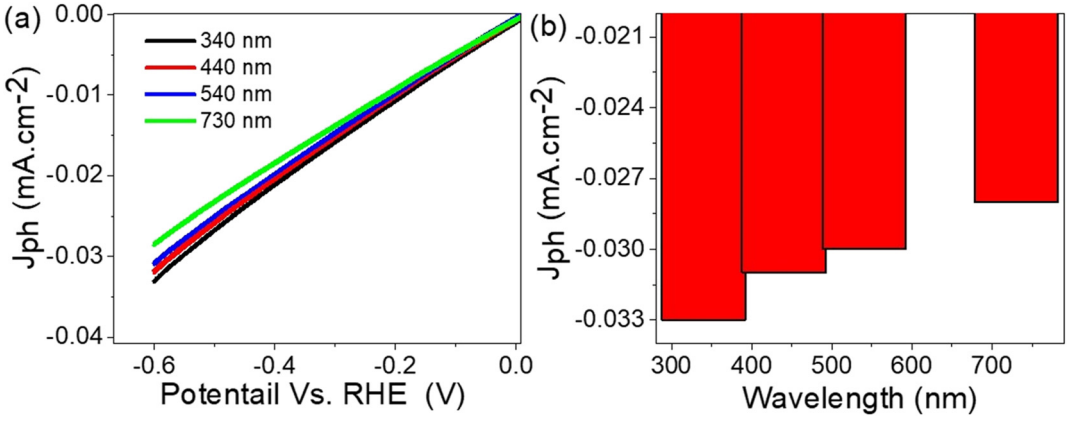

Figure 5: Green hydrogen generation using the fabricated Ag_2S/P2MA thin film nanoribbon photocathode with natural Red Sea water under different photon energies: (a) linear sweep voltammetry and (b) corresponding values derived from this curve.

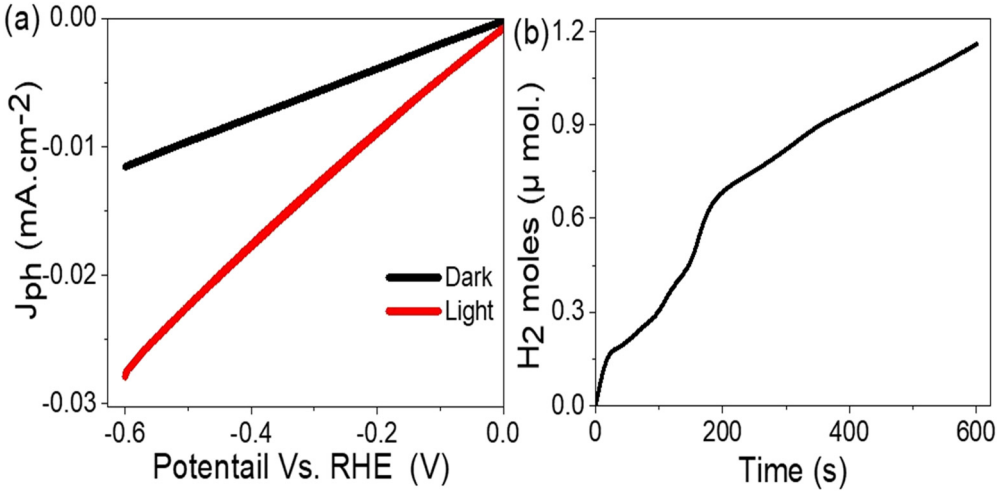

Figure 6: (a) Green hydrogen generation using the fabricated Ag_2S/P2MA thin film nanoribbon photocathode with artificial seawater under different photon energies, and (b) the estimated hydrogen moles produced using Faraday's law.

Table 2: Comparison of hydrogen moles generated by the Ag_2S/P2MA thin film nanoribbon photocathode with the results from previous studies

Photocathode	Electrolyte	H_2 moles generated (μmol/h cm^2)
Polypyrrole/NiO_x [32]	Wastewater	2
Polyaniline/PbI_2 [33]	Sanitation water	5
Poly(*m*-toluidine)/roll-GO [34]	Sewage water	4
WO_2I_2/polypyrrole [35]	Seawater	5.2
Ag_2S/P2MA nanoribbon photocathode (this study)	Natural seawater	14

electrolysis was applied. Figure 6(b) shows that the amount of hydrogen generated is approximately 14 μmol/h cm^2. This is a significant amount of hydrogen produced from a thin film surface, surpassing the hydrogen output estimated in previous studies involving polypyrrole/NiO_x [32] or polyaniline/PbI_2 [33], which has an H_2 gas rate of about 2–5 μmol/cm^2 h.

The Ag_2S/P2MA thin film photocathode, therefore, emerges as a highly promising candidate for hydrogen provided from Red Sea water. Its efficiency, coupled with the potential for mass production and low cost, makes it a strong contender for industrial utilization (Table 2).

4 Conclusions

The Ag_2S-P2MA nanoribbon photocathodes are synthesized using a one-pot method involving the oxidation of 2-mercaptoaniline with $(NH_4)_2S_2O_8$ and $AgNO_3$. Characterization *via* SEM and TEM reveals that these nanocomposites exhibit nanoribbon structures, typically measuring a width of 150 nm and lengths ranging from 500 to 1,000 nm. Optical absorbance analyses indicate that the composite absorbs light up to 780 nm, with a bandgap of 2.16 eV.

These photocathodes are engineered for hydrogen gas generation through water splitting using two distinct electrolytes: natural Red Sea water and artificial seawater devoid of heavy metals. The Ag_2S-P2MA nanoribbon photocathodes demonstrate stable performance, producing hydrogen at a rate of 12 μmol/cm^2 h. In natural seawater, the light-induced J_{ph} and J_o values are −0.033 and −0.017 mA/cm^2, respectively, while in artificial seawater, these values are −0.027 and −0.012 mA/cm^2, respectively. Given their cost-effectiveness, stability, and potential for large-scale production, these photocathodes are well-suited for commercial electrode applications across various industrial sectors.

Acknowledgments: Researchers Supporting Program Number (RSPD2025R845), King Saud University, Riyadh, Saudi Arabia.

Funding information: Researchers Supporting Program Number (RSPD2025R845), King Saud University, Riyadh, Saudi Arabia.

Author contributions: Mohamed Rabia – methodology and writing; Eman Aldosari – writing, supervision, and project management; Aimaro Sanna and Osama Farid – supervision and revising the data. All authors have accepted responsibility for the entire content of this manuscript and approved its submission.

Conflict of interest: The authors state no conflict of interest.

Data availability statement: All data generated or analyzed during this study are included in this published article.

References

[1] Morales-Guio CG, Tilley SD, Vrubel H, Graẗzel M, Hu X. Hydrogen evolution from a copper(I) oxide photocathode coated with an amorphous molybdenum sulphide catalyst. Nat Commun. 2014;5(1):1–7.

[2] Fan JL, Li Z, Huang X, Li K, Zhang X, Lu X, et al. A net-zero emissions strategy for China's power sector using carbon-capture utilization and storage. Nat Commun. 2023;14(1):1–16.

[3] Rabia M, Elsayed AM, Alnuwaiser MA. Highly morphological behavior AgI/P1HP intercalated with iodide ions in the polymer chains as a promising photocathode for the hydrogen generation from Red Sea water. Opt Quantum Electron. 2024;56:1–16.

[4] Aldosari E, Rabia M, Zhang Q. Highly photocatalytic materials based on the decoration of poly(O-chloroaniline) with molybdenum trichalcogenide oxide for green hydrogen generation from Red Sea water. Green Process Synth. 2024;13:20240040.

[5] Oshiro K, Fujimori S. Limited impact of hydrogen co-firing on prolonging fossil-based power generation under low emissions scenarios. Nat Commun. 2024;15(1):1–11.

[6] Purvis G, Šiller L, Crosskey A, Vincent J, Wills C, Sheriff J, et al. Generation of long-chain fatty acids by hydrogen-driven bicarbonate reduction in ancient alkaline hydrothermal vents. Commun Earth Environ. 2024;5(1):1–9.

[7] Giovanniello MA, Cybulsky AN, Schittekatte T, Mallapragada DS. The influence of additionality and time-matching requirements on the emissions from grid-connected hydrogen production. Nat Energy. 2024;9:197–207.

[8] Zhu W, Yang L, Liu F, Si Z, Huo M, Li Z, et al. Metal Ni nanoparticles in-situ anchored on CdS nanowires as effective cocatalyst for boosting the photocatalytic H_2 production and degradation activity. J Alloy Compd. 2024;973:172747.

[9] Askari MB, Salarizadeh P. Superior catalytic performance of $NiCo_2O_4$ nanorods loaded rGO towards methanol electro-oxidation and hydrogen evolution reaction. J Mol Liq. 2019;291:111306.

[10] Zhao W, Luo L, Cong M, Liu X, Zhang Z, Bahri M, et al. Nanoscale covalent organic frameworks for enhanced photocatalytic hydrogen production. Nat Commun. 2024;15(1):1–11.

[11] de Kleijne K, Huijbregts MAJ, Knobloch F, van Zelm R, Hilbers JP, de Coninck H, et al. Worldwide greenhouse gas emissions of green hydrogen production and transport. Nat Energy. 2024;9:1139–52.

[12] Tsao CW, Narra S, Kao JC, Lin YC, Chen CY, Chin YC, et al. Dual-plasmonic Au@Cu_7S_4 yolk@shell nanocrystals for photocatalytic hydrogen production across visible to near infrared spectral region. Nat Commun. 2024;15(1):1–13.

[13] Kountouris I, Bramstoft R, Madsen T, Gea-Bermúdez J, Münster M, Keles D. A unified European hydrogen infrastructure planning to support the rapid scale-up of hydrogen production. Nat Commun. 2024;15(1):1–13.

[14] Rabia M, Elsayed AM, Alnuwaiser MA. Promising porous spherical PbI_2/poly-2-aminobenzenethiol nanocomposite as a photocathode for hydrogen generation from Red Sea water. Phys Scr. 2024;99:085044.

[15] Moradi-Alavian S, Kazempour A, Mirzaei-Saatlo M, Ashassi-Sorkhabi H, Mehrdad A, Asghari E, et al. Promotion of hydrogen evolution from seawater via poly(aniline-co-4-nitroaniline) combined with 3D nickel nanoparticles. Sci Rep. 2023;13:1–10.

[16] Al-saeedi SI. Photoelectrochemical green hydrogen production utilizing ZnO nanostructured photoelectrodes. Micromachines. 2023;14(5):1047.

[17] Azzam EMS, Abd El-Salam HM, Aboad RS. Kinetic preparation and antibacterial activity of nanocrystalline poly(2-aminothiophenol). Polym Bull. 2019;76:1929–47.

[18] Shaban M, Rabia M, El-Sayed AMA, Ahmed A, Sayed S. Photocatalytic properties of PbS/graphene oxide/polyaniline electrode for hydrogen generation. Sci Rep. 2017;7:14100.

[19] Zhao C, Yu Z, Xing J, Zou Y, Liu H, Zhang H, et al. Effect of ag_2s nanocrystals/reduced graphene oxide interface on hydrogen evolution reaction. Catalysts. 2020;10:1–12.

[20] Arulraj A, Ilayaraja N, Rajeshkumar V, Ramesh M. Direct synthesis of cubic shaped Ag_2S on Ni mesh as binder-free electrodes for energy storage applications. Sci Rep. 2019;9:3–10.

[21] Dwech MH, Aadim KA, Hamid LA. Influence of laser energy on the characteristics of Ag2S/ITO thin films solar cell prepared by PLD technique. AIP Conf Proc. 2020;2213:020147.

[22] Patel H, Joshi J. Green and chemical approach for synthesis of Ag_2O nanoparticles and their antimicrobial activity. J Sol-Gel Sci Technol. 2023;105:814–26.

[23] Burton AW, Ong K, Rea T, Chan IY. On the estimation of average crystallite size of zeolites from the Scherrer equation: A critical evaluation of its application to zeolites with one-dimensional pore systems. Microporous Mesoporous Mater. 2009;117:75–90.

[24] Lim DJ, Marks NA, Rowles MR. Universal Scherrer equation for graphene fragments. Carbon. 2020;162:475–80.

[25] Abdelazeez AAA, Ben A, Trabelsi G, Alkallas FH, Alfaify S, Shkir M, et al. Reproducible preparation of thin graphene films using a green and efficient liquid-phase exfoliation method for applications in photovoltaics. Coatings. 2023;13(9):1628.

[26] Brown AM, Sundararaman R, Narang P, Goddard WA, Atwater HA. Nonradiative plasmon decay and hot carrier dynamics: Effects of phonons, surfaces, and geometry. ACS Nano. 2016;10:957–66.

[27] Dunseath O, Smith EJW, Al-Jeda T, Smith JA, King S, May PW, et al. Studies of Black Diamond as an antibacterial surface for Gram Negative bacteria: the interplay between chemical and mechanical bactericidal activity. Sci Rep. 2019;9(1):1–10.

[28] Haryński Ł, Olejnik A, Grochowska K, Siuzdak K. A facile method for Tauc exponent and corresponding electronic transitions determination in semiconductors directly from UV–Vis spectroscopy data. Opt Mater. 2022;127:112205.

[29] Dolgonos A, Mason TO, Poeppelmeier KR. Direct optical band gap measurement in polycrystalline semiconductors: A critical look at the Tauc method. J Solid State Chem. 2016;240:43–8.

[30] Bohra H, Tan SY, Shao J, Yang C, Efrem A, Zhao Y, et al. Narrow bandgap thienothiadiazole-based conjugated porous polymers: from facile direct arylation polymerization to tunable porosities and optoelectronic properties. Polym Chem. 2016;7:6413–21.
[31] Anju PV, Deivasigamani P. Structurally engineered ion-receptor probe immobilized porous polymer platform as reusable solid-state chromogenic sensor for the ultra-trace sensing and recovery of mercury ions. J Hazard Mater. 2023;454:131431.
[32] Atta A, Negm H, Abdeltwab E, Rabia M, Abdelhamied MM. Facile fabrication of polypyrrole/NiO_x core-shell nanocomposites for hydrogen production from wastewater. Polym Adv Technol. 2023;34(5):1633–41.
[33] Hadia NMA, Khalafalla MAH, Salam FMA, Ahmed AM, Shaban M, Almuqrin AH, et al. Conversion of sewage water into H_2 gas fuel using hexagonal nanosheets of the polyaniline-assisted deposition of PbI2 as a nanocomposite photocathode with the theoretical qualitative ab-initio calculation of the H_2O splitting. Polymers. 2022;14:2148.
[34] Helmy A, Rabia M, Shaban M, Ashraf AM, Ahmed S, Ahmed AM. Graphite/rolled graphene oxide/carbon nanotube photoelectrode for water splitting of exhaust car solution. Int J Energy Res. 2020;44:7687–97.
[35] Rabia M, Aldosari E, Elsayed AM, Sanna A, Farid O Highly porous network of tungsten (VI) oxide-iodide/polypyrrole nanocomposite photocathode for the green hydrogen generation. Opt Quantum Electron. 2024;56(6):1–17.